J Mater Sci (2016) 51:6474–6487

Solidification microstructures in Ag_3Sn–Cu_3Sn pseudo-binary alloys

Haibo Yu[1], Yu Sun[1], S. Pamir Alpay[1], and Mark Aindow[1,*]

[1] *Department of Materials Science and Engineering, Institute of Materials Science, University of Connecticut, Unit 3136, 97 North Eagleville Road, Storrs, CT 06269-3136, USA*

Received: 12 March 2016
Accepted: 30 March 2016
Published online: 11 April 2016

ABSTRACT

The solidification microstructures in three alloys from the Ag_3Sn–Cu_3Sn pseudo-binary section in the Ag–Cu–Sn system have been studied using a combination of X-ray diffraction, electron microscopy, differential scanning calorimetry, and quenching experiments. The three alloys have Ag:Cu ratios of 50:50, 40:60, and 30:70. In each case, the as-cast structures exhibit the equilibrium phases θ-Ag_3Sn and ε_1-Cu_3Sn, with a little η-Cu_6Sn_5. There is no evidence of the metastable high-temperature phases that are so prevalent in as-cast structures of the corresponding binary alloys. The differential scanning calorimetry data obtained on heating the alloy samples are consistent with the transformations expected on the basis of the published ternary Ag–Cu–Sn diagrams. It is proposed that the solidification microstructures observed experimentally in such alloys must correspond to the nucleation of the high-temperature phases being kinetically limited upon cooling for these compositions. This leads to the direct formation of the equilibrium low-temperature phases by eutectic-type co-operative growth.

Introduction

The Ag–Cu–Sn system has attracted a great deal of attention, largely because Sn-rich alloys in this system are good candidates for Pb-free solders [1, 2]. There are no ternary intermetallic phases formed in the Ag–Cu–Sn system [3], but the diversity of binary phases leads to complex phase equilibria for some ternary compositions. There is an Sn-rich ternary eutectic that forms the basis of most solder formulations: this occurs at around 218 °C with a composition of 3.5 % Ag, 1.1 % Cu and 95.4 % Sn (atomic percent) [4]. Upon solidification, a three-phase mixture is formed comprising: β-Sn, θ-Ag_3Sn and η-Cu_6Sn_5 (phases are designated following the notation adopted by Chang et al. [5]). These latter phases are the most Sn-rich intermetallics in the corresponding binary systems. In the binary Ag-Sn system, there is also a close-packed hexagonal phase ε_2-Ag_5Sn. In the binary Cu-Sn system, there is one other low-temperature intermetallic phase, ε_1-Cu_3Sn, and three high-temperature phases (β-$Cu_{13}Sn_3$, γ-Cu_4Sn, and δ-$Cu_{41}Sn_{11}$).

The phases θ-Ag_3Sn and ε_1-Cu_3Sn are iso-structural and exhibit the geometrically close-packed

Address correspondence to E-mail: m.aindow@uconn.edu

orthorhombic Cu_3Ti-type structure ($D0_a$, space group *Cmcm*) [6–8], although non-stoichiometric ε_1-Cu_3Sn can deviate from the ideal $D0_a$ structure due to displacive lattice modulations or periodic faulting [9, 10]. Both phases play an important role in microelectronic applications utilizing lead-free solders, where they can be present as minority strengthening phases in the solder alloy and can form as reaction products at solder/substrate interfaces [11–14]. Thin interfacial films of these phases can promote the formation of a good metallurgical bond at the solder joint, but coarsened interfacial phases can lead to embrittlement and to thermal fatigue or creep failures [15–17]. These $D0_a$ compounds are also of interest because they are found in dental amalgams as part of complex phase mixtures [6, 18, 19].

Studying the properties of these $D0_a$ phases is challenging because the phase equilibria make the production of good quality single-phase samples very difficult. In the binary Ag-Sn system, the θ-Ag_3Sn phase forms via a rather sluggish peritectic reaction between Sn-rich liquid and the ε_2-Ag_5Sn phase [20]. In binary Cu-Sn alloys, ε_1-Cu_3Sn forms via congruent ordering from the cubic BiF_3-type γ-Cu_4Sn phase, which is itself a peritectic reaction product [21]. There has been some success in producing bulk single-phase θ-Ag_3Sn and ε_1-Cu_3Sn samples by casting followed by long-term annealing [22]. These samples were used to measure the elastic properties, hardness, and indentation fracture toughness of the phases, but concerns remain about segregation and/or oxidation effects on measurements from material produced via this route.

In the present study, we selected three alloys with compositions that lie on the Ag_3Sn–Cu_3Sn pseudo-binary and examined the solidification microstructures to evaluate the extent to which the complex phase equilibria can be avoided. X-ray diffraction (XRD) and scanning electron microscopy (SEM) data from as-cast samples of the three alloys gave the unexpected result that the θ-Ag_3Sn and ε_1-Cu_3Sn phases can form directly from the melt via a eutectic-type solidification process. Differential scanning calorimetry (DSC), heat-treatment/quenching, and transmission electron microscopy (TEM) experiments were then used to investigate the discrepancy between the observed microstructures and those expected on the basis of the published ternary Ag–Cu-Sn phase diagram. It is inferred from these data that the nucleation of intermediate phases such as ε_2-Ag_5Sn in the melt is suppressed even at very modest cooling rates, leading to the formation of the phase mixtures observed experimentally.

Materials and experimental methods

Three $(Ag,Cu)_3Sn$ alloy compositions were selected for this study as shown in Table 1. These are referred to as the 50:50, 40:60, and 30:70 alloy samples, where the designations refer to the ratio of the atomic percentages of Ag and Cu in the respective alloys. Cylindrical ingots, 25 mm in diameter, were produced by ACI Alloys, Inc. (San Jose, CA) for each of the alloys from high-purity elemental starting materials by arc-melting and casting under argon gas.

Samples for XRD and SEM analyses were obtained by slicing disks of about 2 mm in thickness from the cylindrical ingots. These samples were ground using successively finer grades of SiC abrasive papers, and were then polished using colloidal alumina suspension. The XRD studies were performed on the polished surfaces using a Bruker AXS D2 Phaser diffractometer equipped with a 30 kV Cu Kα source and a Lynxeye detector. The data were obtained by scanning over a 2θ range of 20–60° at a scan speed of 0.02°/s for a total time of 2.5 h. These data were analyzed by comparison with standard International Centre for Diffraction Data (ICDD) files. Backscattered electron (BSE) SEM images and energy-dispersive X-ray spectrometry (EDXS) data were obtained from the polished sample surfaces in a FEI Teneo LoVac SEM equipped with an EDAX Octane silicon drift detector (SDD) EDXS system.

Small pieces were broken from each alloy, and samples with an approximate weight of 10 mg were used for DSC analyses. The initial analyses were performed in a TA Instruments SDT Q600 under a purified argon atmosphere using a heating rate of 10 °C/min. To identify the processes occurring at each significant event in the DSC signatures, parallel heating and quenching experiments were performed in a TA Instruments DSC 2920, which allows for

Table 1 Nominal compositions of the three alloys

Alloy #	Composition (at.%)			Composition (wt%)		
	Ag	Cu	Sn	Ag	Cu	Sn
50:50	37.5	37.5	25.0	43.0	25.4	31.6
40:60	30.0	45.0	25.0	35.7	31.6	32.7
30:70	22.5	52.5	25.0	27.8	38.2	34.0

samples to be removed rapidly from the apparatus. The heating conditions were matched to those of the initial DSC analyses, i.e., 10-mg samples were heated at 10 °C/min under purified argon to the required temperatures. The samples were then removed and immediately quenched in water at room temperature. The quenched samples were mounted in cold-setting epoxy resin loaded with a conductive filler of Ni powder, ground and polished to a mirror finish, and the microstructures were examined using BSE imaging and EDXS analyses in the SEM.

For selected samples, analyses of microstructural details were performed by TEM. The TEM specimens were prepared by focused ion beam (FIB) milling techniques from polished sample surfaces using an FEI Helios Nanolab G3 dual-beam FIB instrument, which is equipped with a flip-stage and a scanning transmission electron microscopy (STEM) detector for improved final thinning. A 3-μm-thick Pt layer was deposited onto the polished surfaces in situ to protect the surface of the TEM specimen during ion milling. This deposition was accomplished in two steps: the first 1 μm of Pt was deposited using the electron beam to crack the organometallic Pt precursor, and the remaining 2 μm of Pt was deposited using the ion beam. In the initial stages of the milling process, the accelerating voltage used for the ion column was 30 kV and the ion beam currents were reduced iteratively to a value of 28 pA. During the final milling process, the accelerating voltage for the ion column was reduced to 5 kV and the ion beam current used was reduced to 15 pA to avoid excessive Ga^+ implantation and beam damage. The FIB-cut slices were mounted onto Mo grids and attached at one edge to avoid the re-deposition of the grid materials onto the sample surface during final thinning. The TEM specimens were examined in an FEI Tecnai T12 TEM and in an FEI Talos F200X S/TEM operating at accelerating voltages of 120 and 200 kV, respectively. The latter instrument is equipped with a Super-X SDD EDXS system, which allows for rapid acquisition of spectrum images for elemental mapping.

Results

Microstructure of the as-cast alloys

Producing fine powders from these alloys proved to be particularly challenging, and so XRD data were obtained in Bragg-Bretano geometry from the polished surfaces of disks cut from the ingots. Representative examples of the data obtained from the three alloys are shown in Fig. 1, where the counts are plotted on a logarithmic scale to better show the low intensity peaks. We note that the relative intensities of the peaks (but not the peak positions) varied from scan to scan for each sample indicating that there are pronounced effects from the grain size and/or preferred grain orientations in these ingots. The majority of the XRD peaks correspond to those expected for the $D0_a$ phases θ-Ag_3Sn ($a_0 = 0.597$ nm, $b_0 = 0.478$ nm, $c_0 = 0.518$ nm [6]) and ε_1-Cu_3Sn ($a_0 = 0.549$ nm, $b_0 = 0.432$ nm, $c_0 = 0.474$ nm [7]). There are also minor peaks corresponding to the long-period superstructure polymorph of Cu_3Sn ($a_0 = 0.553$ nm, $b_0 = 4.775$ nm, $c_0 = 0.432$ nm, space group *Cmcm* [9][1]) in the XRD data from the 50:50 alloy. This long-period polymorph of Cu_3Sn is now widely accepted as the equilibrium form, but requires extended annealing to develop fully (e.g., [23]). We note that the absence of such peaks in the data from the 40:60 and 30:70 alloys does not necessarily demonstrate that this polymorph is not present in these alloys since most of the peaks from this polymorph of Cu_3Sn overlap with those from the $D0_a$ ε_1 structure. Minor peaks from the hexagonal η-Cu_6Sn_5 phase ($a_0 = 0.419$ nm, $c_0 = 0.509$ nm, space group $P6_3/mmc$ [24]) were observed in each of the alloys, although here again some of the peaks from this phase overlap with those from the phases ε_1-Cu_3Sn and θ-Ag_3Sn.

The microstructures of the as-cast alloys were investigated using BSE imaging and EDXS analysis on metallographic sections in the SEM. Examples of typical BSE SEM images from the three alloys are presented in Fig. 2. There is strong compositional contrast in such images, and EDXS point analyses were used to confirm that the light and dark regions correspond to the main Ag_3Sn and Cu_3Sn phases, respectively. There are also occasional small gray regions corresponding to the Cu_6Sn_5 phase, and examples of these are shown in the insets to each micrograph. In each case, it was found that these phases are not pure stoichiometric compounds, but instead there is some solubility of Cu in Ag_3Sn, and of Ag in Cu_3Sn and Cu_6Sn_5. The mean compositions

[1] It is important to note that the conventions used to define the axes in the $D0_a$ and long-period polymorphs are different. Thus, the *b* axis of the long-period structure lies parallel to *c* in the conventional description of the $D0_a$ structure, and b_0 (superstructure) ≈ 10 c_0 ($D0_a$).

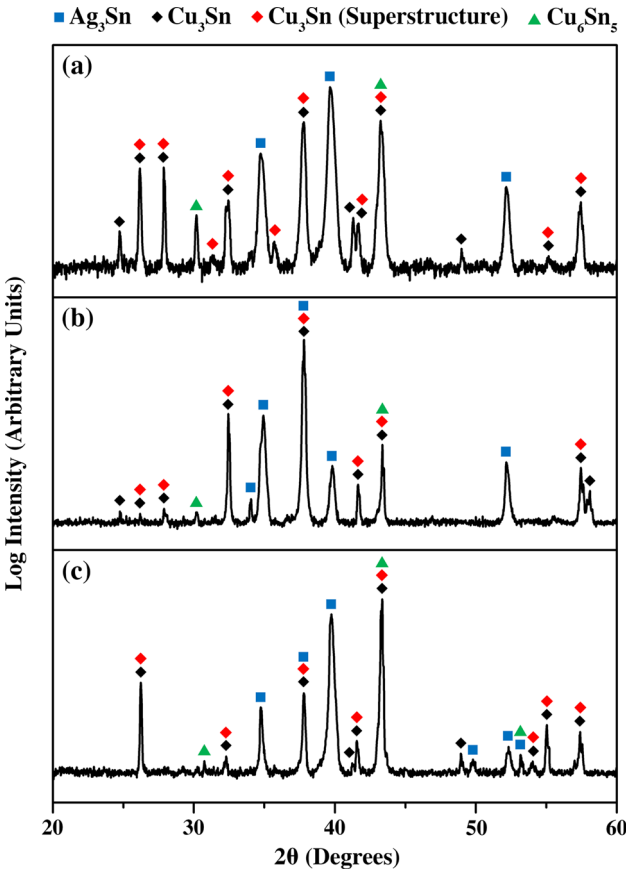

Figure 1 XRD data obtained from as-cast samples of the alloys: **a** 50:50; **b** 40:60; **c** 30:70.

for these majority phases as measured by EDXS are given in Table 2. These values were obtained from the raw Ag L, Cu K, and Sn L signals using library standards with e-ZAF corrections. It can be seen that the phase compositions are rather similar in the three alloys and thus the main effect of the differences in alloy composition is a difference in the volume fractions of the phases. Image analysis was performed on BSE images such as those shown in Fig. 2 and the mean volume fractions of Cu_3Sn obtained were 42, 52, and 64 % for the 50:50, 40:60, and 30:70 alloys, respectively. Since the volume fraction of the Cu_6Sn_5 phase is less than 2 % in each case, the Ag_3Sn phase constitutes most of the remainder of the as-cast microstructures. There is also a transition in the morphology of the phases. In the 50:50 alloy, there is a bimodal size distribution for the Cu_3Sn phase with larger features (several μm across) resembling dendrite arms, and regions of much more finely divided features (<1 μm) that are reminiscent of eutectic micro-constituents. In the 40:60 and 30:70 alloys, the

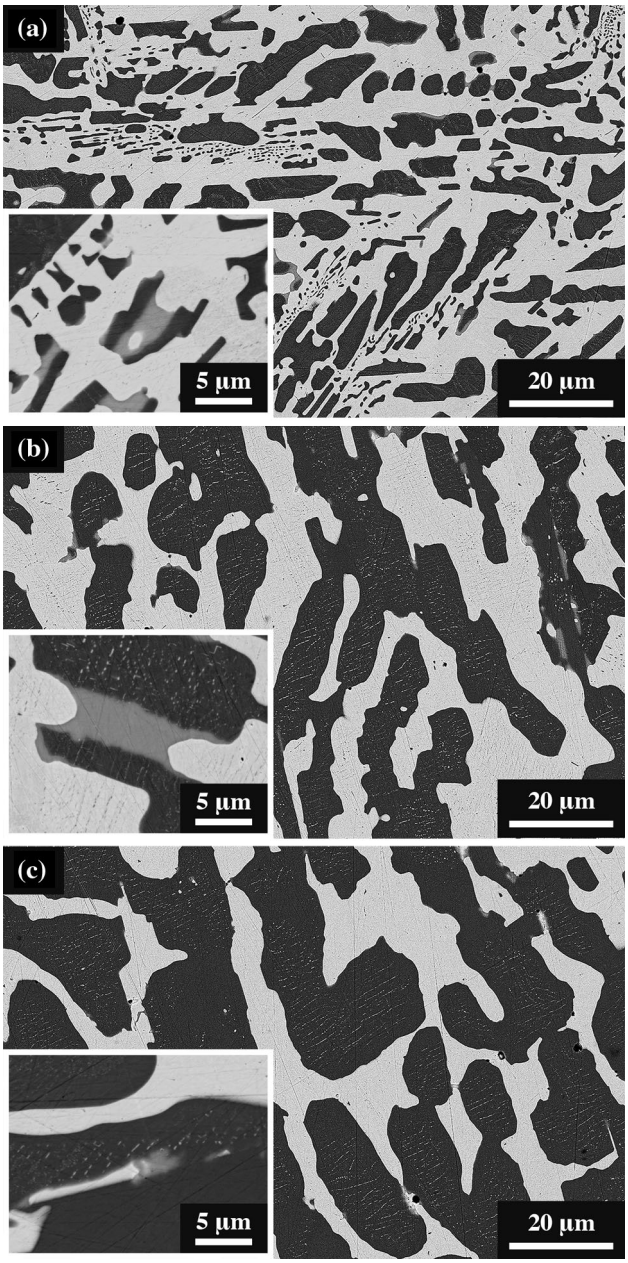

Figure 2 Representative BSE SEM images obtained from as-cast samples of the alloys: **a** 50:50; **b** 40:60; **c** 30:70.

Table 2 Compositions of the phases in the as-cast alloys measured using EDXS in the SEM

Alloy #	Ag_3Sn (at.%)			Cu_3Sn (at.%)			Cu_6Sn_5 (at.%)		
	Ag	Cu	Sn	Ag	Cu	Sn	Ag	Cu	Sn
50:50	68.1	4.8	27.1	3.2	73.4	23.4	1.2	55.6	43.2
40:60	68.0	5.2	26.8	3.2	73.6	23.2	1.1	55.9	43.0
30:70	66.1	7.0	26.9	2.7	73.9	23.4	*	*	*

* The regions of Cu_6Sn_5 phase in the 30:70 alloy were too small to measure accurately by EDXS

majority phases adopt a more uniform blocky morphology, although in both cases there are still occasional regions that show a more finely divided structure.

These data suggest that the mixture of θ-Ag_3Sn and ε_1-Cu_3Sn phases may form directly from the melt, rather than via reactions involving high-temperature phases such as ε_2-Ag_5Sn or γ-Cu_4Sn. There was no evidence for such intermediate phases, or indeed any compositional gradients within the major phases, and both of these effects might have been expected if the phases were formed via the transformation paths that occur in the binary systems. Moreover, as explained in the Discussion section, this is not what one would expect on the basis of the published ternary phase diagram. The DSC and heat-treatment/quenching studies described below were performed to investigate these phenomena.

DSC analyses

The thermal characteristics of these alloys were determined by heating 10 mg samples of the as-cast materials from room temperature to 750 °C at 10 °C/min. In each case, the alloys underwent a series of endothermic processes between 350 and 650 °C, and representative DSC data for the temperature range 300–700 °C are shown in Fig. 3. All three alloys exhibit a small endothermic trough at 355 °C, and much larger sharp troughs at 482 and 531 °C. The alloys also exhibit a fourth, somewhat broader trough. The temperature for this fourth trough varies with composition from 561 to 593 and 618 °C for the 50:50, 40:60, and 30:70 alloys, respectively. These data were repeatable with scans on duplicate samples exhibiting essentially identical trough temperatures and shapes. Furthermore, all of the processes associated with these troughs were found to be reversible. Samples of each alloy were heated from room temperature to 750 °C, cooled to room temperature in the DSC apparatus, and then heated to 750 °C again. The troughs observed upon re-heating showed no significant differences from those in the original scans. For the 50:50 alloy, additional experiments were performed in which samples were heated from room temperature to 400, 500, and 545 °C (i.e., just past the first, second and third troughs, respectively), cooled to room temperature in the DSC apparatus, and then re-heated to the end-point temperature. In each case, the data obtained on re-heating were indistinguishable from those obtained in the initial heating scan. Thus, the thermal events observed in the DSC scans are reversible, both individually and in sequence.

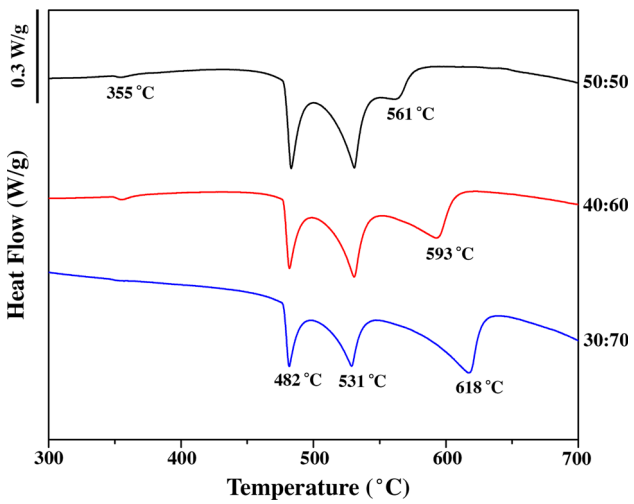

Figure 3 Plots of DSC heat flow data obtained from as-cast alloy samples at a heating rate of 10 °C/min.

To identify the transformations associated with these processes, additional 10-mg samples of each alloy were heated from room temperature to set-points of 400, 500, 545, and 600 °C in a separate DSC apparatus. Upon reaching the set-point, the samples were removed rapidly from the apparatus and quenched into water. The set-points of 400 and 500 °C lie between the invariant troughs at 355, 482, and 531 °C in each sample. The set-point of 545 °C lies between the invariant trough at 531 °C and the fourth trough, whose temperature varies from one sample to another. The set-point of 600 °C is the maximum temperature achievable in this apparatus and lies above the fourth trough for the 50:50 and 40:60 alloys, but below this trough for the 30:70 alloy. The microstructural data obtained from these quenched specimens are described in the sections below.

Microstructures of the quenched 50:50 alloy samples

Examples of BSE SEM images from the quenched 50:50 alloy samples are presented in Fig. 4. The sample quenched from 400 °C (Fig. 4a) exhibits a very similar morphology to that observed in the as-cast 50:50 alloy (Fig. 2a). The only significant difference is the disappearance of the Cu_6Sn_5 phases. The microstructure in the sample quenched from 500 °C

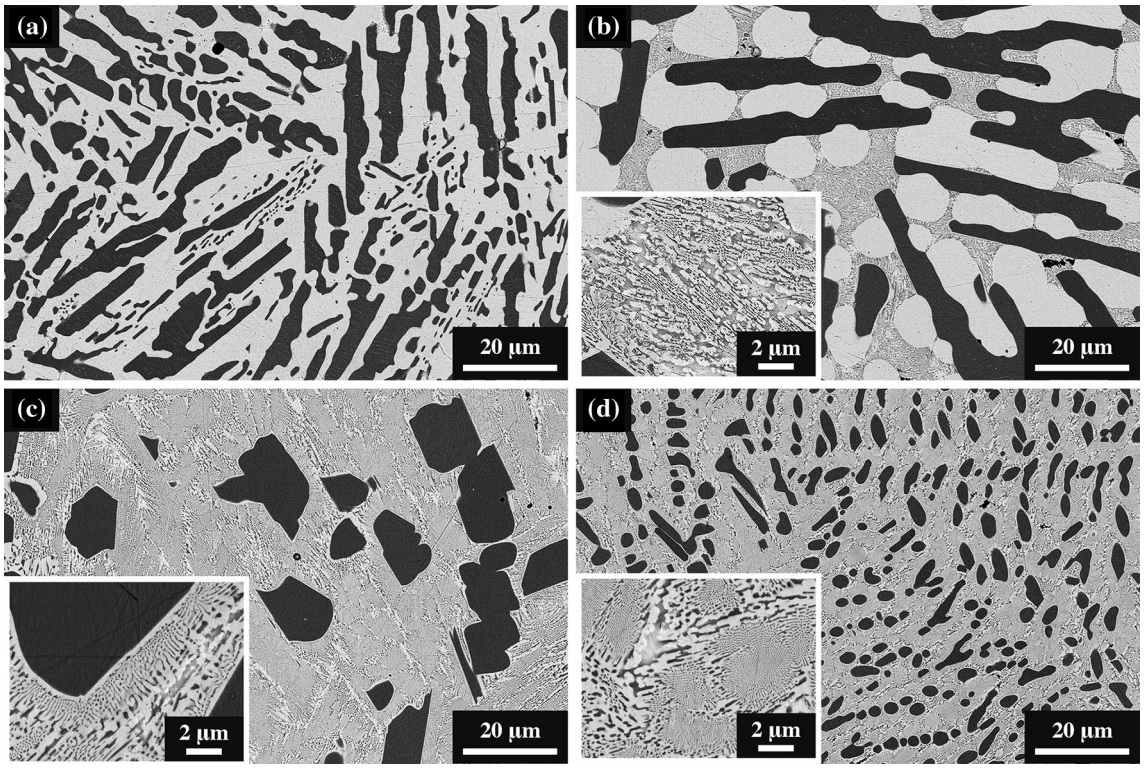

Figure 4 Representative BSE SEM images obtained from 50:50 alloy samples quenched to room temperature from: **a** 400 °C; **b** 500 °C; **c** 545 °C; **d** 600 °C.

was rather different (Fig. 4b) with somewhat coarser Ag_3Sn and Cu_3Sn grains surrounded by a complex phase mixture. The morphology of this mixture is shown at higher magnification in the inset to the figure. The mean volume fractions of the micro-constituents were measured from such images as 40.4 % Ag_3Sn, 37.3 % Cu_3Sn, and 22.3 % of the phase mixture. For the samples quenched from 545 and 600 °C, however, there are only two micro-constituents present: Cu_3Sn grains and a finely divided phase mixture. In both cases, the volume fraction of the Cu_3Sn phase is similar (22.6 and 24.1 vol.%, respectively), but the phase morphologies and sizes are very different. In the sample quenched from 545 °C, the Cu_3Sn is coarser (up to 50 µm across) and more angular. In the sample quenched from 600 °C, the Cu_3Sn is much finer (up to 5 µm across) and more globular. Mean compositions measured by EDXS analysis from the micro-constituents in the four quenched 50:50 alloy samples are presented in Table 3. The compositions of the Ag_3Sn and Cu_3Sn phases are fairly consistent throughout, although there is some minor variation in the Cu and Ag contents of these phases, respectively. The most dramatic differences are in the composition of the phase mixture. The mixture in the sample quenched from 500 °C contains significantly less Ag and more Sn than that in the samples quenched from 545 and 600 °C. In these latter two samples, the EDXS data are very similar suggesting that the phase mixture present is the same.

Table 3 Compositions (in at.%) measured using EDXS in the SEM from the microstructural constituents in the 50:50 alloy samples quenched from set-point temperatures, T

T (°C)	Ag_3Sn			Cu_3Sn			Phase Mixture		
	Ag	Cu	Sn	Ag	Cu	Sn	Ag	Cu	Sn
400	67.1	6.4	26.5	1.5	75.4	23.1	–	–	–
500	69.4	8.2	22.4	2.7	74.1	23.2	37.0	27.3	35.7
545	–	–	–	2.7	74.0	23.3	43.1	29.6	27.3
600	–	–	–	3.3	73.2	23.5	43.8	28.9	27.3

The details of the phase mixtures were investigated by S/TEM analysis on FIB-cut TEM specimens from these micro-constituents in the samples quenched from 500, 545, and 600 °C. A set of data from one such experiment on the sample quenched from

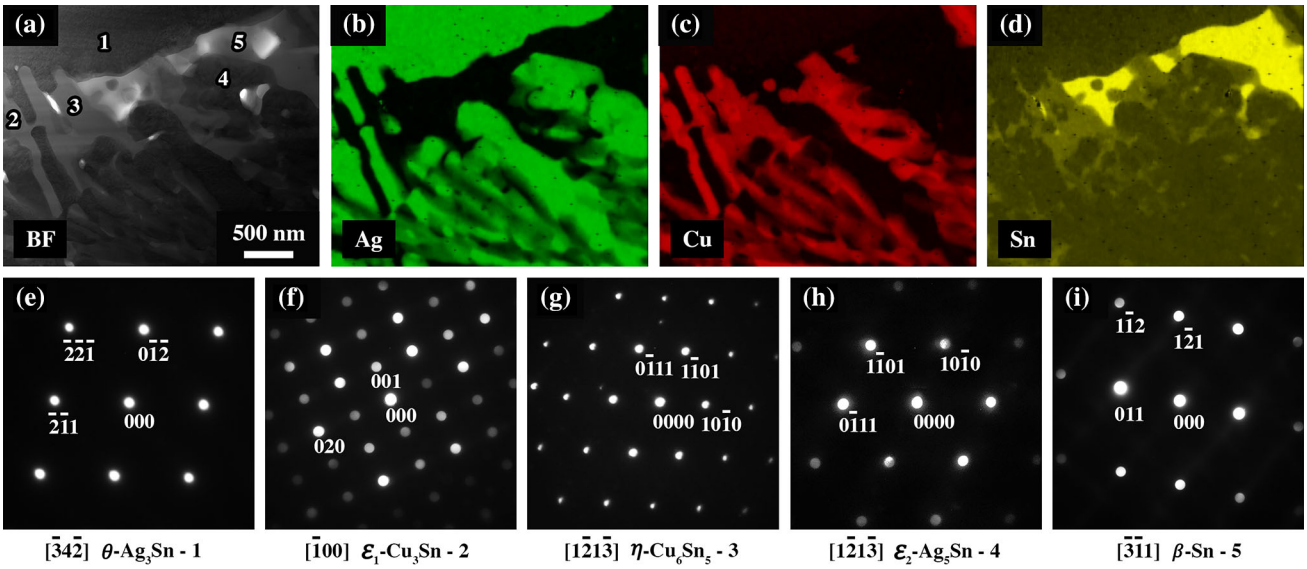

Figure 5 S/TEM data obtained from the complex phase mixture in the 50:50 alloy sample quenched from 500 °C: **a** BF STEM image; **b**–**d** compositional maps obtained from the region in (**a**) showing the distribution of Ag, Cu, and Sn, respectively; **e** SADP from region 1 in (**a**); (**f**–**i**) microdiffraction patterns from regions 2, 3, 4, and 5 in (**a**), respectively. The patterns in (**e**–**i**) are presented at the same camera length.

500 °C is shown in Fig. 5. The bright field (BF) STEM image in Fig. 5a shows a large Ag_3Sn grain at the top left (labeled 1) with smaller grains from the complex phase mixture across the rest of the field of view. The compositional variation was revealed by spectrum imaging in which full spectra were collected at each point in the scan, and these were analyzed by performing a standard-less quantification using the Ag L, Cu K, and Sn L peaks at each point. Thus, the maps shown in Fig. 5b–d are compositional maps (rather than raw X-ray maps) and the intensities in these maps are proportional to the Ag, Cu, and Sn contents, respectively. Based upon these data, four different phases were detected in the mixture and an example of each is labeled (2-5) in Fig. 5a. The phases were identified by tilting the sample until zone axis patterns were obtained from a grain of each phase. Examples of the diffraction data are shown in Fig. 5e–i. The selected-area diffraction pattern (SADP) in Fig. 5e was obtained from the large Ag_3Sn grain at 1 in Fig. 5a; this corresponds to a $[\bar{3}4\bar{2}]$ zone axis pattern (ZAP) from the θ-Ag_3Sn phase. The grains in the phase mixture were too small to give clear SADPs, so instead micro-diffraction patterns were obtained with a convergent probe and a small condenser aperture. Examples of micro-diffraction ZAPs from the grains labeled 2–5 in Fig. 5a are shown in Figs. 5f–i, respectively. These are indexed as the $[\bar{1}00]$ ZAP for ε$_1$-Cu_3Sn, the $[12\bar{1}3\bar{]}$ ZAP for η-Cu_6Sn_5, the $[12\bar{1}3\bar{]}$ ZAP for the hexagonal ε$_2$-Ag_5Sn phase ($a_0 = 0.29658$ nm, $c_0 = 0.47842$ nm, space group $P6_3/mmc$ [20]), and the $[\bar{3}\bar{1}1]$ ZAP for the tetragonal β-Sn phase ($a_0 = 0.582$ nm, $c_0 = 0.318$ nm, space group $I4_1/amd$ [25]). We note that while these patterns are presented at the same scale (effective camera length), they were obtained at different sample orientations and no conclusions could be drawn about the presence, or otherwise, of any orientation relationships between the phases.

Similar experiments on FIB-cut TEM specimens from the samples quenched from 545 and 600 °C revealed much simpler phase mixtures comprising alternating lamellae of the θ-Ag_3Sn and ε$_1$-Cu_3Sn phases. An example of a data set obtained from the sample quenched from 600 °C is shown in Fig. 6. A BF STEM image and the corresponding Ag, Cu and Sn maps are given in Figs. 6a–d, respectively. The SADP in Fig. 6e was obtained from the area shown in Fig. 6a, and Fig. 6f is an indexed schematic of this pattern. The pattern corresponds to overlay of the [142] ZAPs from the θ-Ag_3Sn and ε$_1$-Cu_3Sn phases in the orientation relationship:

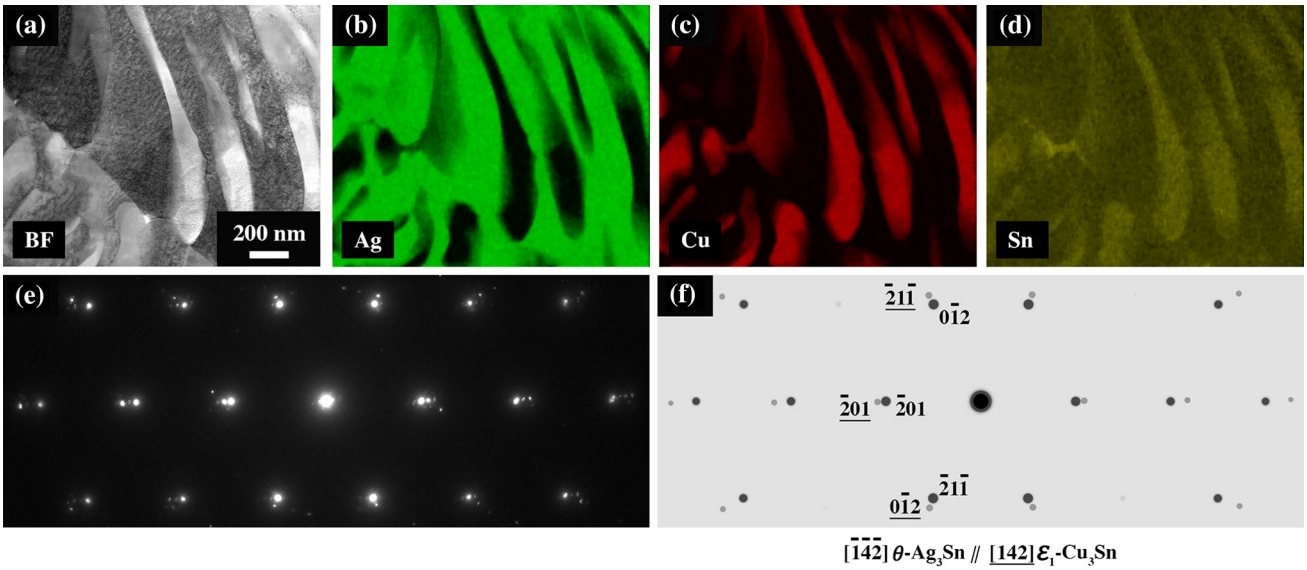

Figure 6 S/TEM data obtained from the eutectic micro-constituent in the 50:50 alloy sample quenched from 600 °C: **a** BF STEM image; **b**–**d** compositional maps obtained from the region in (**a**) showing the distribution of Ag, Cu, and Sn, respectively; **e** SADP obtained from the region shown in (**a**); **f** indexed schematic of the SADP in (**e**).

$[\bar{1}\bar{4}\bar{2}]\ Ag_3Sn\ //\ [142]\ Cu_3Sn$

$(\bar{2}01)Ag_3Sn\ //(\bar{2}01)Cu_3Sn$

$(2\bar{2}3)Ag_3Sn\ //(\bar{2}2\bar{3})Cu_3Sn$

Since the SADP in Fig. 6e includes contributions from several Ag_3Sn and Cu_3Sn lamellae, the phases must be arranged in colonies with well-defined orientations between the layers. Such characteristics are typical of eutectic solidification of phases mixtures with similar structures and modest differences in lattice parameters. We note that similar data were obtained from the phase mixtures in the sample quenched from 545 °C. Further work is underway in an attempt to understand the reasons for the adoption of this orientation relationship in the phase mixture.

Microstructures of the quenched 40:60 and 30:70 alloy samples

A representative selection of BSE SEM images obtained from the 40:60 and 30:70 alloy samples quenched from 500, 545, and 600 °C is shown in Fig. 7. The mean compositions of the micro-constituents in the quenched samples were measured using EDXS in the SEM and these data are summarized in Table 4. We note that, as for the 50:50 alloy, quenching from 400 °C produced no significant microstructural changes other than the disappearance of the Cu_6Sn_5 phases, and only very minor changes in the compositions of the Ag_3Sn and Cu_3Sn phases. The images from these samples are not included in Fig. 7.

The phase distribution in the 40:60 and 30:70 alloy samples quenched from 500 °C (Figs. 7a, b, respectively) is similar to that in the corresponding 50:50 alloy sample (Fig. 4b). There are coarse Ag_3Sn and Cu_3Sn grains plus regions of a complex phase mixture, which are shown at higher magnification in the insets to the figures. The volume fractions of the phase mixtures are significantly lower than that in the 50:50 alloy, at around 8 and 3 % in the 40:60 and 30:70 alloy samples, respectively. The mean compositions of these regions were also different in each alloy, and indeed from region to region in the same sample, suggesting that the compositions and/or proportions of the phases present in such regions vary somewhat.

For the 40:60 and 30:70 alloy samples quenched from 545 °C, only two micro-constituents are observed in the BSE SEM images (Fig. 7c, d, respectively): coarse Cu_3Sn grains and a fine phase mixture that resembles a eutectic. This is very similar to the microstructure observed for the 50:50 alloy quenched from this temperature (Fig. 4c). In contrast to the

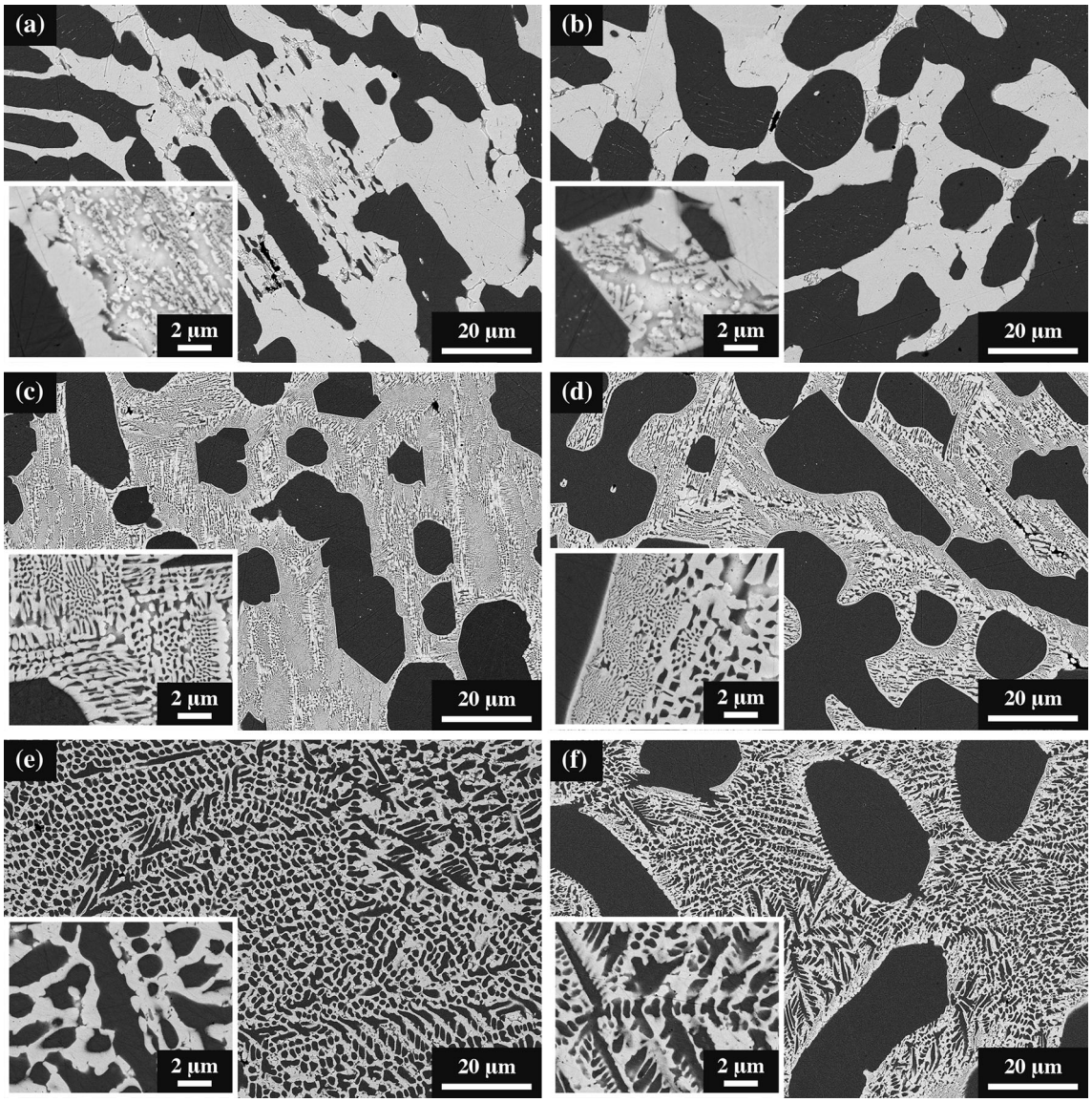

Figure 7 Representative BSE SEM images obtained from the 40:60 (**a**,**c**,**e**) and 30:70 alloy (**b**,**d**,**f**) samples quenched from: **a**,**b** 500 °C; **c**,**d** 545 °C; **e**,**f** 600 °C.

Table 4 Compositions (in at.%) measured using EDXS in the SEM from the microstructural constituents in the 40:60 and 30:70 alloy samples quenched from set-point temperatures, T

Alloy	T (°C)	Ag_3Sn			Cu_3Sn			Phase mixture		
		Ag	Cu	Sn	Ag	Cu	Sn	Ag	Cu	Sn
40:60	400	67.8	5.8	26.4	3.4	73.0	23.6	–	–	–
	500	69.4	7.4	23.2	2.6	74.1	23.3	28.8	18.4	52.8
	545	–	–	–	2.8	74.1	23.1	43.9	28.7	27.4
	600	–	–	–	–	–	–	26.8	48.1	25.1
30:70	400	66.5	7.3	26.2	3.0	74.0	23.0	–	–	–
	500	69.7	7.6	22.7	2.4	74.3	23.3	35.3	22.9	41.8
	545	–	–	–	2.8	73.9	23.3	44.5	29.4	26.1
	600	–	–	–	2.6	74.4	23.0	27.3	47.9	24.8

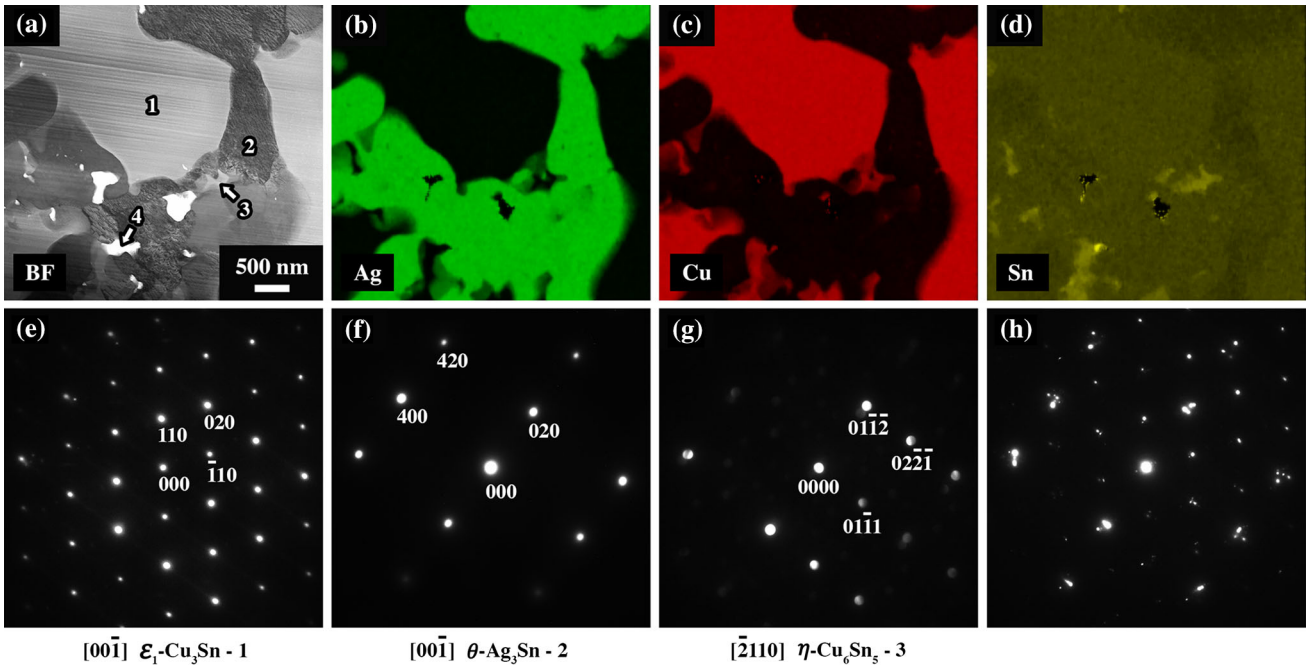

Figure 8 S/TEM data obtained from the phase mixture in the 40:60 alloy sample quenched from 600 °C: **a** BF STEM image; **b**–**d** compositional maps obtained from the region in (**a**) showing the distribution of Ag, Cu, and Sn, respectively; **e**,**f** SADPs from regions 1 and 2 in (**a**), respectively; (**g**) micro-diffraction pattern from region 3 in (**a**); **h** SADP obtained from an area including regions 1 and 2 in (**a**). The patterns in (**e**–**h**) are presented at the camera length.

samples quenched from 500 °C, the compositions of the micro-constituents in these samples were very consistent from region to region. Moreover, as can be seen from the values in Tables 3 and 4, the compositions of these regions are extremely close to one another in the 50:50, 40:60, and 30:70 alloy. This is consistent with the phase mixture in the 40:60 and 30:70 alloy samples being the same combination of θ-Ag_3Sn and ε_1-Cu_3Sn observed in the 50:50 alloy. Under these circumstances, the differences in the overall alloy composition must be accommodated by differences in the volume fractions of the micro-constituents. The mean volume fractions of the Cu_3Sn micro-constituent (as opposed to the total volume fractions of the Cu_3Sn phase including the Cu_3Sn in the phase mixture) measured for the 50:50, 40:60, and 30:70 alloy samples quenched from 545 °C were 22.6, 36.6, and 49.8 %, respectively.

The 40:60 alloy sample quenched from 600 °C exhibited a microstructure consisting of a homogeneously distributed phase mixture (Fig. 7e), which is significantly coarser than the mixtures in the samples quenched from 500 and 545 °C (Fig. 7a, c, respectively). The morphology of this phase mixture is also different from those observed upon quenching from these lower temperatures; in this case there are dark "feathery" dendritic structures with finer bright features between the dendrite arms. As expected, the composition of the mixture measured by EDXS corresponds closely to the nominal composition of the alloy. For the 30:70 alloy sample quenched from 600 °C, two micro-constituents are observed in the BSE SEM images (Fig. 7f): coarse Cu_3Sn grains and a phase mixture with a similar composition and morphology to, albeit somewhat finer than, that in the corresponding 40:60 alloy sample.

Although the phases mixtures in the 40:60 and 30:70 alloy samples quenched from 500 and 545 °C resemble those in the corresponding 50:50 alloy samples, the feathery dendritic mixtures in the samples quenched from 600 °C are clearly different. Here again, the characters of the phases in these mixtures were investigated by S/TEM analysis on FIB-cut TEM specimens, and a set of data from one such experiment on the 40:60 alloy sample quenched from 600 °C is shown in Fig. 8. The BF STEM image in Fig. 8a reveals a lobe from a dendrite (region 1) surrounded by a mixture of finer grains. The corresponding Ag, Cu, and Sn maps (Figs. 8b–d) and the [00$\bar{1}$] SADP from region 1 (Fig. 8e) show that the

dendrite is composed of the ε_1-Cu_3Sn phase. Most of the grains in the surrounding mixture are θ-Ag_3Sn, and an example of a $[00\bar{1}]$ SADP from this phase is shown in Fig. 8f. There are some finer η-Cu_6Sn_5 grains, such as region 3 from which the $[\bar{2}110]$ microdiffraction pattern in Fig. 8g was obtained. There are also some Sn-rich pockets, such as region 4, that are too small to give clear ZAPs, but are presumably β-Sn phase. We note that some of the θ-Ag_3Sn regions adjacent to the ε_1-Cu_3Sn dendrites appeared to exhibit a simple low-index orientation relationship:

$[00\bar{1}]$ Ag_3Sn // $[00\bar{1}]$ Cu_3Sn

$(010)Ag_3Sn$ //$(010)Cu_3Sn$

$(100)Ag_3Sn$ //$(100)Cu_3Sn$

Regions 1 and 2 in Fig. 8a are an example of this, as demonstrated in and the SADP obtained with the field limiting aperture surrounding these regions (Fig. 8h). The differences between the $[00\bar{1}]$ ZAPs for these isostructural compounds arise because the 110- and 200-type reflections in the $D0_a$ structure are chemically sensitive. These reflections are extremely weak in Ag_3Sn because the atomic scattering factors for Ag and Sn are very similar, as one might expect for elements with an atomic number difference of only 3. For Cu_3Sn, however, these reflections are fairly strong due to large differences in the atomic scattering factors. This is why the 110- and 200-type reflections from Cu_3Sn are visible in Fig. 8h, but those from Ag_3Sn are not.

Discussion

The phase equilibria in the Ag–Cu–Sn system have been described by Hari Kumar and Kubaschewski [26, 27]. While recent attention has upon the Sn-rich corner of this system, the understanding of the transformations for alloys with the Sn-lean compositions considered here is based upon the earlier work of Gebhardt and Petzow [28] and Fedorov et al. [29] who produced isothermal sections and isopleths at 5–25 wt% Sn. On this basis, one would expect the following transformation sequence upon cooling:

$$\mathrm{L} \rightarrow \mathrm{L} + \epsilon_1 \rightarrow L + \epsilon_1 + \epsilon_2 \rightarrow \mathrm{L} + \epsilon_1 + \theta \rightarrow \epsilon_1 + \theta + \eta$$

Thus, the phases present in the as-cast structure correspond to those predicted by the equilibrium phase diagram (i.e., mainly ε_1-Cu_3Sn and θ-Ag_3Sn, with a little η-Cu_6Sn_5). Moreover, the DSC troughs observed upon heating can be reconciled with the processes expected from the phase diagram. The small invariant trough at 355 °C corresponds to the peritectic reaction:

$$\eta \rightarrow \epsilon_1 + \mathrm{L}$$

As such, the η-Cu_6Sn_5 phase is absent from the microstructures in samples quenched from 400 °C (e.g., Figure 4a). The larger invariant trough at 482 °C corresponds to the peritectic reaction:

$$\theta \rightarrow \epsilon_2 + \mathrm{L}$$

This results in more complex microstructures in samples quenched from 500 °C (Figs. 4b, 7a, b). There are large grains of untransformed ε_1-Cu_3Sn and θ-Ag_3Sn, plus a complex phase mixture of ε_2-Ag_5Sn with ε_1-Cu_3Sn, η-Cu_6Sn_5, and β-Sn, which form when the Cu- and Sn-rich liquid freezes around the ε_2 transformation product. Clearly, the presence of large regions of untransformed θ-Ag_3Sn indicates that the peritectic reaction is kinetically limited at these temperatures and heating rates. The second large invariant trough at 531 °C corresponds to the congruent melting:

$$\epsilon_1 + \epsilon_2 \rightarrow \mathrm{L}$$

As such, in samples heated to 545 °C, there is only liquid plus rather blocky ε_1-Cu_3Sn phase present. Upon quenching from 545 °C, a fine eutectic mixture of ε_1-Cu_3Sn and θ-Ag_3Sn forms (Figs. 4b, 7a, b).

Lastly, there is a broad trough whose temperature depends on the alloy composition. This lies at 561, 593, and 618 °C for the 50:50, 40:60, and 30:70 alloys, respectively. The trough corresponds to the melting of the ε_1-Cu_3Sn phase, and therefore the temperatures at which these troughs occur are approximately those for the liquidus surface at these compositions. The samples quenched from 600 °C exhibit rather different microstructures. For the 50:50 alloy, the alloy is fully liquid at this temperature and quenching produces a refined microstructure (Fig. 4d) with primary ε_1-Cu_3Sn and the same $\varepsilon_1 + \theta$ eutectic as in the samples quenched from 545 °C. For the 40:60 alloy, 600 °C is just beyond the trough and it is not clear whether a homogeneous liquid would be produced. Upon quenching from 600 °C, we observe a mixture of feathery ε_1-Cu_3Sn dendrites surrounded by grains of θ-Ag_3Sn, plus smaller grains of η-Cu_6Sn_5 and yet

smaller pockets of β-Sn (Fig. 7e). For the 30:70 alloy, 600 °C is below the trough and one would expect liquid plus coarse ε_1-Cu_3Sn phase to be present. Upon quenching from 600 °C, the liquid solidifies into a phase mixture with a similar composition and morphology (if somewhat finer) to that for the 40:60 alloy (Fig. 7f).

While the transformations that occur upon heating are consistent with the published ternary phase diagrams, most of the solidification microstructures (both in as-cast and in quenched samples) do not correspond to what one might expect on this basis or based upon previous work on binary alloys (e.g., [22]). In the latter case, extended annealing was required to eliminate segregation effects and regions of high-temperature phases such as ε_2-Ag_5Sn and γ-Cu_4Sn when producing samples of θ-Ag_3Sn and ε_1-Cu_3Sn, respectively. No such effects were observed in the samples considered here. The ε_2-Ag_5Sn phase was only observed in samples heated through the peritectic point at 482 °C and then quenched-in before this phase melts into a eutectic liquid at 531 °C. In all other samples, the phases present are θ-Ag_3Sn, ε_1-Cu_3Sn, and in some cases η-Cu_6Sn_5 plus a little β-Sn. The most likely explanation for this is that the *nucleation* of the ε_2-Ag_5Sn phase upon cooling is kinetically limited, and that the formation of this phase is suppressed in favor of the formation of the low-temperature equilibrium phases. It is difficult to prove this for the as-cast samples since the thermal history is not known accurately. As such, it is possible (although rather unlikely) that the ε_2-Ag_5Sn phase forms and is then eliminated completely from the microstructure during slow cooling of the alloy ingots. For the samples quenched from 545 °C, however, there is clearly insufficient time for such processes. The undercooling required to bypass the region of thermodynamic stability for the ε_2-Ag_5Sn phase is only ≈50 °C at these compositions, and so it seems reasonable that one should obtain a eutectic θ-Ag_3Sn + ε_1-Cu_3Sn mixture around the remaining primary ε_1-Cu_3Sn upon cooling. For the samples quenched from 600 °C, the microstructures are different for the three alloys. In the 50:50 alloy the microstructure looks similar to those in the samples quenched from 545 °C with primary ε_1-Cu_3Sn and eutectic θ-Ag_3Sn + ε_1-Cu_3Sn. In the 40:60 alloy a different phase morphology is produced with feathery ε_1-Cu_3Sn dendrites and an inter-dendritic mixture of θ-Ag_3Sn, η-Cu_6Sn_5 and β-Sn. The dendritic morphology and the orientation relationship between the dendrites and some of the adjacent θ-Ag_3Sn grains confirm that the ε_1-Cu_3Sn forms first, rather than co-operatively as in the θ-Ag_3Sn + ε_1-Cu_3Sn eutectic. The driving force for the formation of the ε_1-Cu_3Sn dendrites is presumably the concentration of Cu in the liquid, which is far higher than that at which the eutectic forms. The formation of a phase mixture with a similar composition and morphology in the 30:70 alloy quenched from 600 °C is consistent with this argument.

What is clear is that alloys with these compositions offer an interesting opportunity to study the characteristics and properties of the θ-Ag_3Sn and ε_1-Cu_3Sn phases without needing to perform long-term annealing to eliminate metastable high-temperature phases. The only caveat to such studies would be that the effects of Cu in solid solution in θ-Ag_3Sn, and Ag in ε_1-Cu_3Sn, would need to be taken into account.

Conclusions

The solidification microstructures and phase transformations in $(Ag,Cu)_3Sn$ alloys with Ag:Cu ratios of 50:50, 40:60, and 30:70 have been studied using XRD, electron microscopy, and DSC techniques. The main findings of this work are

(1) The as-cast microstructures contain mainly the θ-Ag_3Sn and ε_1-Cu_3Sn phases with a little η-Cu_6Sn_5. No metastable high-temperature phases or segregation was observed.
(2) The DSC data obtained upon heating at 10 °C/min revealed three invariant processes: one at 355 °C corresponding to η → ε_1 + liquid; one at 482 °C corresponding to θ → ε_2-Ag_5Sn + liquid; and one at 531 °C corresponding to congruent melting of ε_1 + ε_2. A composition-dependent fourth process corresponding to melting of primary ε_1.
(3) Samples quenched from 400 °C contained θ and ε_1 grains but no η phase.
(4) Samples quenched from 500 °C contained coarse θ and ε_1 grains plus a complex phase mixture of ε_1, ε_2, η, and β-Sn.
(5) Samples quenched from 545 °C contained coarse angular ε_1 grains plus a fine eutectic mixture of θ and ε_1.
(6) Samples quenched from 600 °C exhibited more diverse microstructures. The 50:50 alloy sample

contained fine ε_1 grains plus a eutectic mixture of θ and ε_1. The 40:60 alloy sample contained fine feathery ε_1 grains with interdendritic θ, η, and β grains. The 30:70 alloy sample contained coarse ε_1 grains plus a refined version of the phase mixture in the 40:60 alloy sample.

The absence of the ε_2 phase in all but the samples quenched from 500 °C was accounted for on the basis of the nucleation of this phase being suppressed upon cooling giving instead eutectic θ and ε_1, and other phase mixtures. These θ and ε_1 phases are thus formed far more readily than in the corresponding binary alloys, making these ternary compositions good model systems for studying the phases.

Acknowledgements

The microscopy studies were performed in the UConn/FEI Center for Advanced Microscopy and Materials Analysis (CAMMA).

Compliance with ethical standards

Conflict of Interest The authors declare that they have no conflict of interest.

References

[1] Abtew M, Selvaduray G (2000) Lead-free solders in microelectronics. Mater Sci Eng R 27:95–141

[2] Suganuma K (2001) Advances in lead-free electronics soldering. Curr Opin Solid State Mater Sci 5:55–64

[3] Yen YW, Chen SW (2004) Phase equilibria of the Ag-Sn-Cu ternary system. J Mater Res 19:2298–2305

[4] Moon KW, Boettinger WJ (2004) Accurately determining eutectic compositions: the Sn-Ag-Cu ternary eutectic. J. Metals 56:22–27

[5] Chang YA, Goldberg D, Neumann JP (1977) Phase diagrams and thermodynamic properties of ternary Cu-Ag Systems. J Phys Chem Ref Data 6:621–673

[6] Fairhurst CW, Cohen JB (1972) The crystal structure of two compounds found in dental amalgam: Ag_2Hg_3 and Ag_3Sn. Acta Cryst B28:371–378

[7] Burkhardt W, Schubert K (1959) Über messingartige phasen mit A3-verwandter struktur. Z Metallkde 50:442–452

[8] Brooks PL, Gillam E (1970) The ε-phase in the CuSn system. Acta Metal. 18:1181–1185

[9] Watanabe Y, Fujinaga Y, Iwasaki H (1983) Lattice modulation in the long-period superstructure of Cu_3Sn. Acta Cryst B39:306–311

[10] Müller CJ, Lidin S (2014) Cu_3Sn: Understanding the systematic absences. Acta Cryst B70:879–887

[11] Xia Y, Xie X, Xie X, Lu C (2006) Intermetallic compounds evolution between lead-free solder and Cu-based lead frame alloys during isothermal aging. J Mater Sci 41:2359–2364. doi:10.1007/s10853-006-4501-y

[12] Flandorfer H, Saeed U, Luef C, Sabbar A, Ipser H (2007) Interfaces in lead-free solder alloys: enthalpy of formation of binary Ag-Sn, Cu-Sn and Ni-Sn intermetallic compounds. Thermochim Acta 459:34–39

[13] Shen J, Chan YC, Liu SY (2008) Growth mechanism of bulk Ag_3Sn intermetallic compounds in Sn–Ag solder during solidification. Intermetallics 16:1142

[14] Hsu C-M, Chen S-W (2013) Interfacial reactions with and without current stressing at Sn–Co/Ag and Sn–Co/Cu solder joints. J Mater Sci 48:6640–6646. doi:10.1007/s10853-013-7464-9

[15] Kang SK, Choi WK, Shih D-Y, Henderson DW, Gosselin T, Sarkhel A, Goldsmith C, Puttlitz KJ (2003) Ag_3Sn plate formation in the solidification of near-ternary eutectic Sn-Ag-Cu. J Metals 55:61–65

[16] Laurila T, Vuorinen V, Kivilahti JK (2005) Interfacial reactions between lead-free solders and common base materials. Mater Sci Eng R 49:1–60

[17] Ma H (2009) Constitutive models of creep for lead-free solders. J Mater Sci 44:3841–3851. doi:10.1007/s10853-009-3521-9

[18] Mahler DB, Adey JD (1977) Microprobe analysis of a high Cu amalgam alloy. J Dental Res 56:379–384

[19] Hooghan TK, Pinizzotto RF, Watkins JH, Okabe T (1996) Study of a low copper dental amalgam by analytical transmission electron microscopy. J Mater Res 11:2474–2485

[20] Karakaya I, Thompson WT (1987) The Ag-Sn (Silver-Tin) system. Bull Alloy Phase Diagr 8:340–347

[21] Saunders N, Miodownik AP (1990) The Cu-Sn (Copper-Tin) system. Bull Alloy Phase Diagr 11:278–287

[22] Ghosh G (2004) Elastic properties, hardness, and indentation fracture toughness of intermetallics relevant to electronic packaging. J Mater Res 19:1439–1454

[23] Fürtauer S, Li D, Cupid D, Flandorfer H (2013) The Cu-Sn phase diagram, part i: new experimental results. Intermetallics 34:142–147

[24] Gangulee A, Das GC, Bever MB (1973) X-ray-diffraction and calorimetric investigation of compound Cu_6Sn_5. Met Trans 4:2063–2066

[25] Carapella LA, Hultgren R (1942) The ferromagnetic nature of the beta-phase in the copper-manganese-tin system. Trans AIME 147:232–242

[26] Kubaschewski O (1988) Silver–Copper–Tin; MSIT ternary evaluation program, in MSIT Workplace In: Effenberg G (ed) MSI, Materials Science International Services GmbH, Stuttgart, Document ID: 10.16022.1.20

[27] Hari Kumar KC, Kubaschewski O (1988) Ag–Cu–Sn (Silver–Copper–Tin), in non-ferrous metal systems. Part 3 (Landolt-Börnstein: Group IV Physical Chemistry). In: Effenberg G, Ilyenko S (eds), vol 11C3. Materials Science International Services GmbH, Stuttgart, pp 47–62

[28] Gebhardt E, Petzow G (1959) Über den Aufbau des Systems Silber-Kupfer-Zinn. Z Metallkd 50:597–605

[29] Fedorov VN, Osintsev OE, Yushkina ET (1982) Ag–Cu–Sn, in phase diagrams of metallic systems. In: Ageev NV, Petrova LA (eds), vol 26. Acad. Sci. USSR, Moscow, pp 149–150